PROCEEDINGS OF SPIE

SPIEDigitalLibrary.org/conference-proceedings-of-spie

High accurate and efficient electrical impedance tomography for fast brain imaging

Hoang Van Tran, Min Hyuck Kim, Thong Chi Le, Hargsoon Yoon

Hoang Van Tran, Min Hyuck Kim, Thong Chi Le, Hargsoon Yoon, "High accurate and efficient electrical impedance tomography for fast brain imaging," Proc. SPIE 12485, Nano-, Bio-, Info-Tech Sensors, and Wearable Systems 2023, 1248506 (18 April 2023); doi: 10.1117/12.2659172



Event: SPIE Smart Structures + Nondestructive Evaluation, 2023, Long Beach, California, United States

High Accurate and Efficient Electrical Impedance Tomography for Fast Brain Imaging

Hoang Van Tran*a, Min Hyuck Kim b, Thong Chi Le b, Hargsoon Yoon *ab a Center for Materials Research, b Department of Engineering, Norfolk State University, 700 Park Avenue, Norfolk, VA, USA, 23504

* h.v.tran@spartans.nsu.edu
hyoon@nsu.edu

ABSTRACT

Electrical Impedance Tomography (EIT) is a medical imaging technique that reconstructs impedance distribution inside a target object by injecting electrical currents into pairs of electrodes and measuring induced voltages on the remaining electrodes. Since neural signals result from the activity of ion channels causing impedance changes in the cell membrane, EIT can image these neural activities for understanding brain function and medical purposes. In our research, our self-developed electronic prototype board was used to generate high-quality electrical current and collect the data on electrodes with a high sampling rate and bit-resolution. In image reconstruction, a preprocessing data analysis algorithm was newly developed and applied to improve the accuracy of our EIT imaging. The human head has complex anatomical geometry and non-uniform resistivity distribution along with the highly resistive skull, which makes brain-EIT remains challenging inaccurate image reconstruction. To mimic the human head, a multi-layered human head phantom was designed and tested to investigate the effect of the skull structure on imaging. In this presentation, comparison studies for measurements and simulation results will be introduced to discuss the source of errors and improve the accuracy and efficiency of our brain-EIT system.

Keywords: Electrical Impedance Tomography, Brain Imaging, Efficiency, Accuracy

1. INTRODUCTION

Electrical Impedance Tomography (EIT) is a medical imaging technique that allows imaging of the impedance variations inside a volume of interest [1]. EIT is a non-invasive, radiation-free, and low-cost imaging method that other medical imaging methods, like Computed Tomology (CT) and Magnetic Resonance Imaging (MRI), don't possess, although CT and MRI can provide high-resolution body maps. CT scan uses low doses of radiation, although it has not been shown to cause long-term harm, but still contains minor potential harm. MRI, on the other hand, requires a long time to get the results. CT and MRI are expensive, and their portability is very low [2], while the EIT system is portable and has the potential to be more popular.

Although some commercial products have already appeared [3] [4], these devices are used for lung function imaging. EIT still has some key factors that limit the application of EIT in brain imaging, including (1) low skull conductivity and electrode-skin contact impedance, (2) modeling accuracy, (3) reconstruction algorithm, and (4) drive pattern and current density protocols. Despite these limitations, many scientific works proved the potential of EIT in brain imaging applications. Some of the applications that can be mentioned are the localizing epileptic foci using EIT with subdural electrodes [5] [6], imaging, diagnosis, and differentiation of hemorrhagic and ischemic strokes [7] [8], non-invasive monitoring of regional cerebral edema and brain injuries [9] [10] [11].

In this paper, we propose our methods to overcome EIT's limitations, including the essential hardware aspects, mimicking the human head by fabricating a head phantom attached high resistivity skull structure and preprocessing data algorithm. Combining the above methods, plus creating a 3D Finite Element Model (FEM) adapting to the head phantom dimension, and developing Graphic User Interface (GUI), make our system operate highly efficiently and accurately.

The proposed methods are presented in section 2. Therein, our custom-designed electronic board in section 2.1 will emphasize the high-quality analog electrical current source and high sampling rate, bit-resolution Analog-to-Digital Converters (ADCs). The data preprocessing algorithm will be in section 2.2, and the fabrication processes of the multi-layer head phantom will be in section 2.3. The experiment setup and results will be appropriately shown in sections 3 and 4. Section 5 will finalize with a discussion and conclusion.

Nano-, Bio-, Info-Tech Sensors, and Wearable Systems 2023, edited by Jaehwan Kim, Ilkwon Oh, Maurizio Porfiri, Hargsoon Yoon, Proc. of SPIE Vol. 12485, 1248506 ⋅ © 2023 SPIE ⋅ 0277-786X ⋅ doi: 10.1117/12.2659172

2. METHODS

Electrical Impedance Tomography (EIT) is composed of three main components, including EIT image reconstruction algorithms, an electronic prototype board, and a phantom with electrodes attached around the boundary of the sensing domain. Figure 2.1 shows the block diagram of our implemented Electrical Impedance Tomography system utilized for brain imaging. The first component of the system is our custom-designed electronic prototype board that incorporates an alternative electrical current source, multiplexers & microcontrollers, analog-to-digital converters, and a processor with memory. The second component of the system is software functions that operate on a computer, such as data preprocessing and EIT image reconstruction algorithms. The last component is an array of electrodes attached to the human head. Since testing the EIT system on a real human head need more investigation related to safety, the experiment results that are presented in this report were conducted with a multi-layered human head phantom. The following sections will deliver the improvements on each component that contribute to increasing the efficiency and accuracy of image reconstruction.

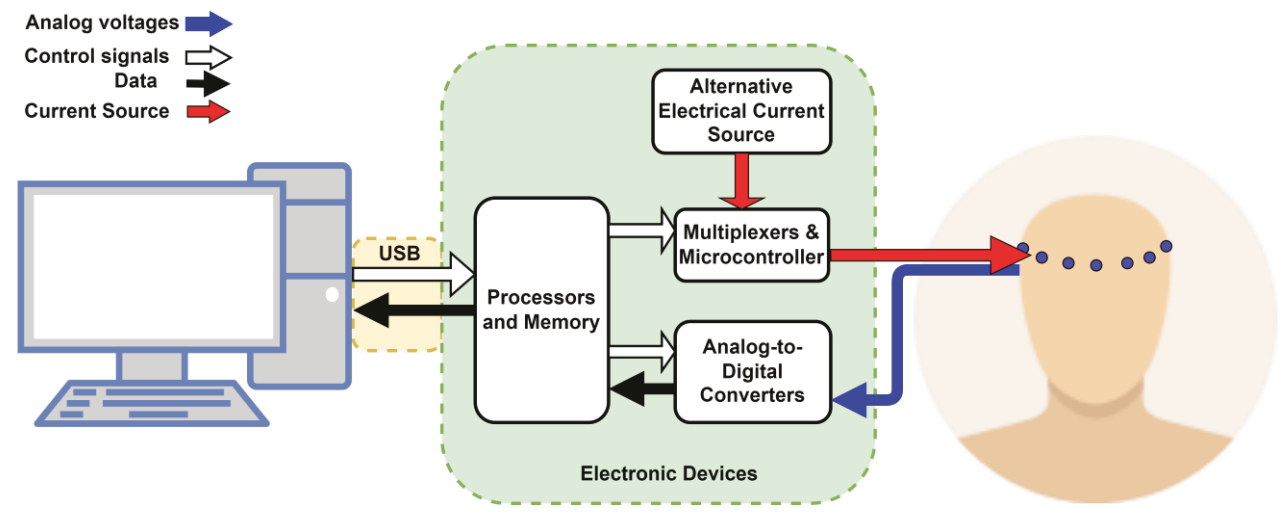


Figure 2.1. Block diagram of Electrical Impedance Tomography system

2.1 Custom-Designed Electronic Prototype Board

As displayed in Figure 2.1, there are four main blocks in the electronic EIT board. The first block is an Alternative Electrical Current Source, which generates a high-quality electrical current. The second block, Analog-to-Digital Converters (ADC), converts analog voltages into digital data, which is transmitted to the Computer by the Processor and Memory, the third block. This block not only sends digital data from ADC to the Computer but also receives control signals from the Computer to configure all components on the board. The final block, Multiplexers & Microcontroller, selects the pair electrodes injected with the current source and synchronizes with other parts using control signals from the Processor & Memory block.



Figure 2.2. The custom-designed electronic prototype board for Neural EIT.

Our custom-designed electronic prototype board was first introduced in [12], which has all components on one board for a size of 15cm x 15 cm. Figure 2.2 shows the board's top view and bottom view, which are marked four important components located on it. This section of the paper will emphasize the importance of the Alternative Electrical Current Source and Analog-to-Digital Converter (ADC) for achieving good reconstruction images. The detail in designing the Analog Electrical Current Source will also be presented, companion with the selection of ADC chips.

2.1.1 High-quality Analog Electrical Current Source

The principle of EIT introduced above uses the electrical current source to inject into the pair of electrodes. For the single-frequency current source method, it is necessary to have a stable, low-noise current source to increase the data quality, improving image reconstruction accuracy later. An analog electrical current source has the advantage of precision and less noise than a digital current source. Figure 2.3 shows the block diagram of our designed current source containing five blocks of circuits. A 3-stage RC phase shift oscillator circuit generates the sinusoid waveform at 1680 Hz. An active high-pass filter at 1000 Hz is used to remove the harmonics at low frequencies. An active low-pass filter at 4000 Hz removes the high-frequencies noises, followed by the voltage attenuation circuit to reduce the magnitude of the waveform before feeding into the improved Howland current source circuits. The output of the current source circuit is at the frequency of 1680 Hz and amplitude of $100 \,\mu\text{A}$.



Figure 2.3. Block diagram of the designed analog electrical current source

To evaluate our designed electrical current source, a 1 k Ω resistor, and a Digilent Analog Discovery 2 kit were used, as shown in Figure 2.4 (a). Figure 2.5 displays the evaluation results of our implemented electrical current source, in which the waveform is displayed at the top of the figure in companion with its measurement values. With the 1 k Ω resister and the 100 μ A amplitude of the current source, the PeaktoPeak value of 200.17 mV and frequency of 1.6791 kHz strongly confirm the high quality of our implemented current source. Although a slight offset of the measured voltage is shown in the Fast Fourier Transform plot, we can easily remove it after getting the data from ADCs and doing some simple digital processing.

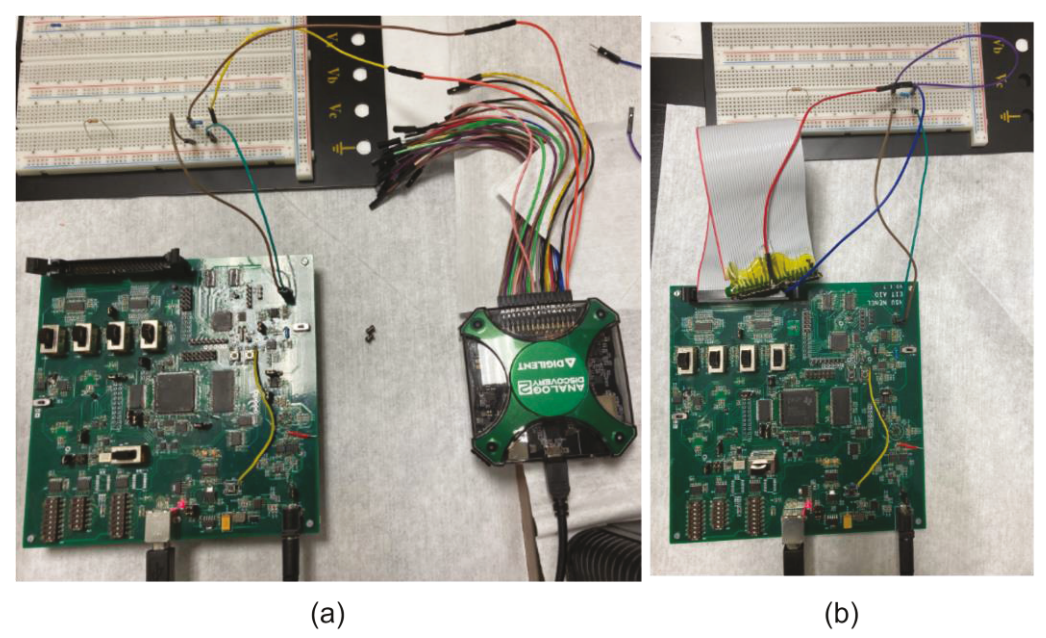


Figure 2.4. Evaluation of electrical current source and Analog-to-Digital Converters setup. (a) - Testing current source with $1 \text{ k}\Omega$ resister and Digilent Analog Discovery 2 kit. (b) Testing ADCs using the designed current source and $1 \text{ k}\Omega$ resistor.

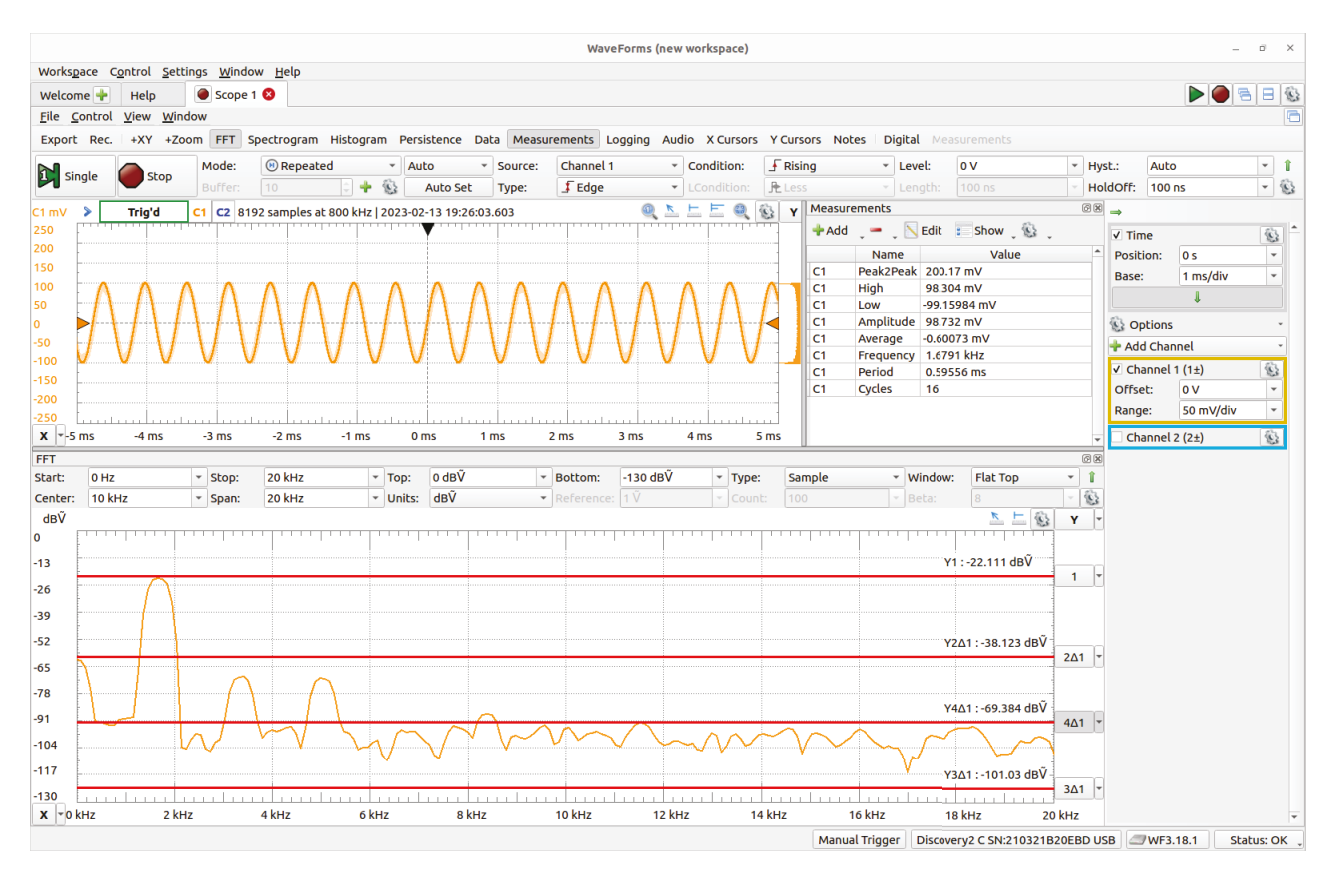


Figure 2.5. Evaluation results of our designed electrical current source.

2.1.2 High sampling rate and bit-resolution of Analog-to-Digital Converters

The Analog-to-Digital Converters were used to measure the induced voltages on the electrodes while the electrical current was injected into the selected pair of electrodes. To achieve a good sensitivity of detecting impedance changes in image reconstruction at the later steps of the EIT system, data acquisition is required to have outstanding accuracy and a high signal-to-noise ratio (SNR). The 24-bit, delta-sigma ($\Delta\Sigma$) ADS1278 ADC was selected to integrate into our custom-designed EIT board, allowing simultaneous sampling of 8 channels in parallel. For having 16 input channels EIT, two ADS1278 chips, which have 8 input channels each, were used in companion with 16 simple RC filters that can provide high-quality data acquisition.

Table 2.1. ADS12	78 operating	mode performa	ince summary [13]	ı

MODE	Max data rate (SPS)	Passband (kHz)	SNR (dB)	Noise (μV _{RMS})	Power/Channel (mW)	Oversampling ratio (f _{MOD} /f _{DATA)}
High-Speed	144351	65742	106	8.5	70	64
High-Resolution	52734	23899	110	5.5	64	128
Low-Power	52734	23899	106	8.5	31	64
Low-Speed	10547	4798	107	8.0	7	64

Table 2.1 summarizes the performance of ADS1278 that have four modes of operation. The High-Speed mode has the highest data rate, 144351 SPS, while the High-Resolution mode has a better Signal-to-Noise Ratio and a data rate of 52734 SPS. There are 8 digital filters inside the ADS1278 that use a multi-stage FIR topology to provide linear with minimal passband ripple and high stopband attenuation. The oversampling ratio of the digital filter (that is, the ratio of

the modulator sampling to the output data rate, or f_{MOD}/f_{DATA}) is a function of the selected mode, in which the High-Resolution mode has a double value in comparison with other modes.

To ensure that the ADCs were effective, a test was performed using the configuration depicted in Figure 2.4(b). Our designed current source we presented above was used in companion with 1 k Ω resistor. All 16 input channels of ADCs measured the induced voltage on the resistor and converted it to digital data. The data was then captured by the processor and memory on the board and sent to a computer for analysis using MATLAB software. The data analysis involved several steps, including reading the binary data file, eliminating the offset voltage, plotting the data for each of the 16 channels for comparison, and performing a Fast Fourier Transform to visualize the frequency spectrum. Figure 2.6 shows the representative data of channels 1, 5, 9, and 16 and two FFT graphs. The pure sinewave on the data graph and the extremely narrow frequency band on the FFT confirmed the accuracy of our system's ADCs.

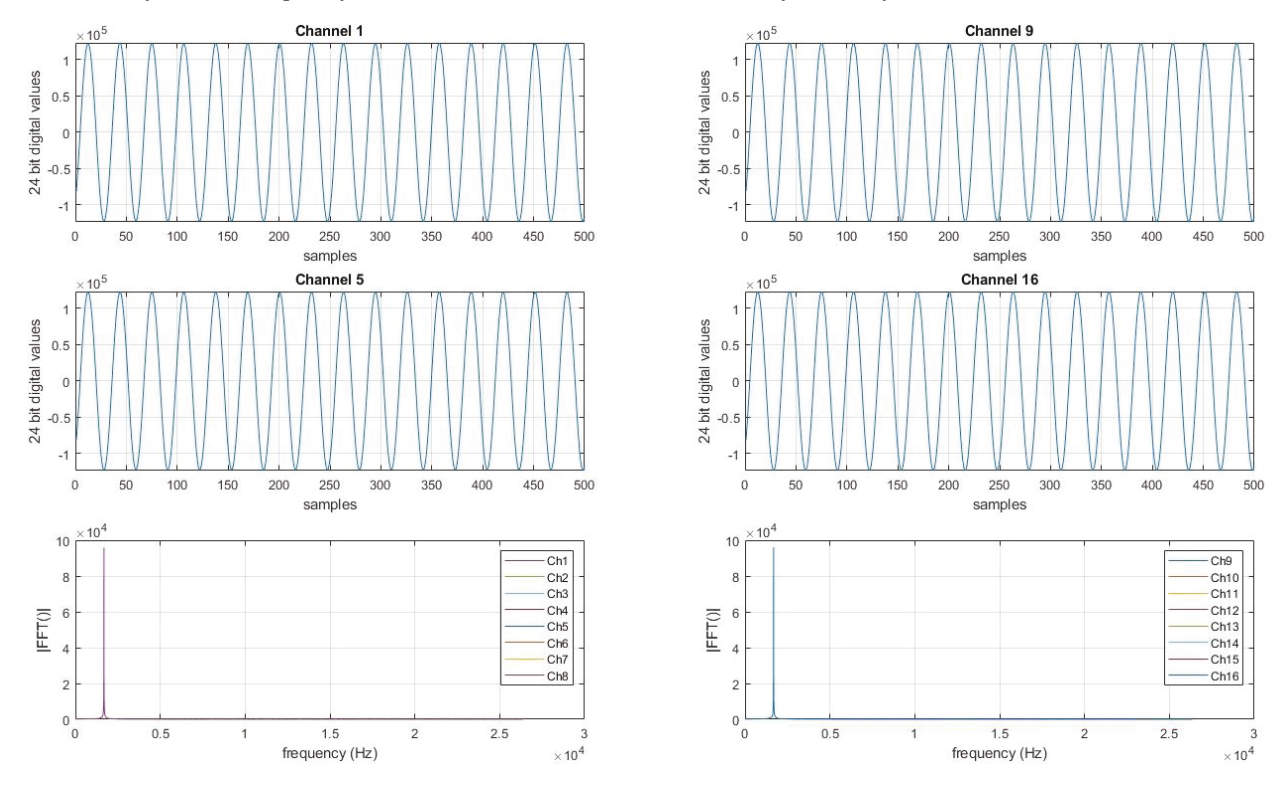


Figure 2.6. Evaluation results of 16 channels data of ADCs.

2.2 Preprocessing Data to Improve the EIT Imaging

The raw data that got from EIT electronic board wasn't ready to feed into the EIT image reconstruction algorithm and needed more preprocessing. Figure 2.7 presents several steps that the raw data need to go through to improve the accuracy of reconstruction images.

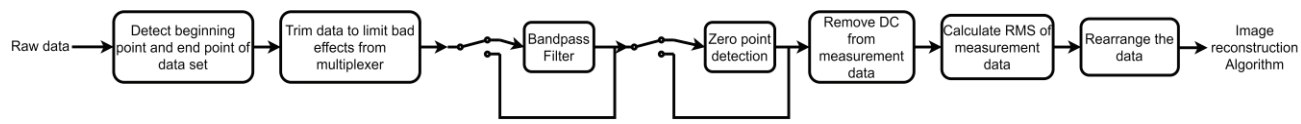


Figure 2.7. Block diagram of preprocessing data process

In the first step, after data was fetched into the program from the binary data file, we needed to detect the beginning of the dataset of one round of 16-channel current injection. By using energy calculation in comparison with the specified threshold, we can determine the data point at which the current source was injected into the first pair of electrodes. The endpoint of the dataset could be calculated by using the sampling rate value, the number of channels of the EIT system, and the duration of the current injection. The second to fourth steps, which were first introduced in [12] by us, have roles in reducing the capacitor charging and discharging effect each time switching the current source and speeding up the

synchronization and collection of data by trimming the data around the multiplexer's switching time and detecting zerocrossing point to capture only two sinewave cycles data. The Band-pass filter was an optional step in between depending on how the noise of the data was. The efficiency of these steps was already proved in [12] and will not mention again in this report. In the fifth and sixth steps, offset values were removed from the measurement data, followed by root-meansquare (RMS) values were calculated. The last step was data arrangement to fit with the input requirements of image reconstruction functions.

2.3 Multi-layered Human Head Phantom

Developing and fabricating the head phantom is necessary to validate the efficiency of our EIT system. The anatomical geometry of the human head is complex, and the skull structure has higher electrical resistance than the scalp and brain tissues, which is challenging with brain EIT. This section will provide a standard procedure to fabricate the head phantom, which is a reproducible, stable, and efficient method.

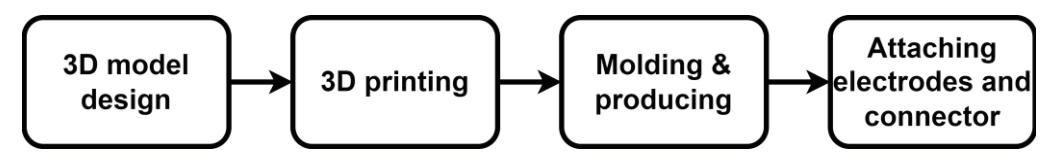


Figure 2.8. Fabrication process in making multi-layered head phantom.

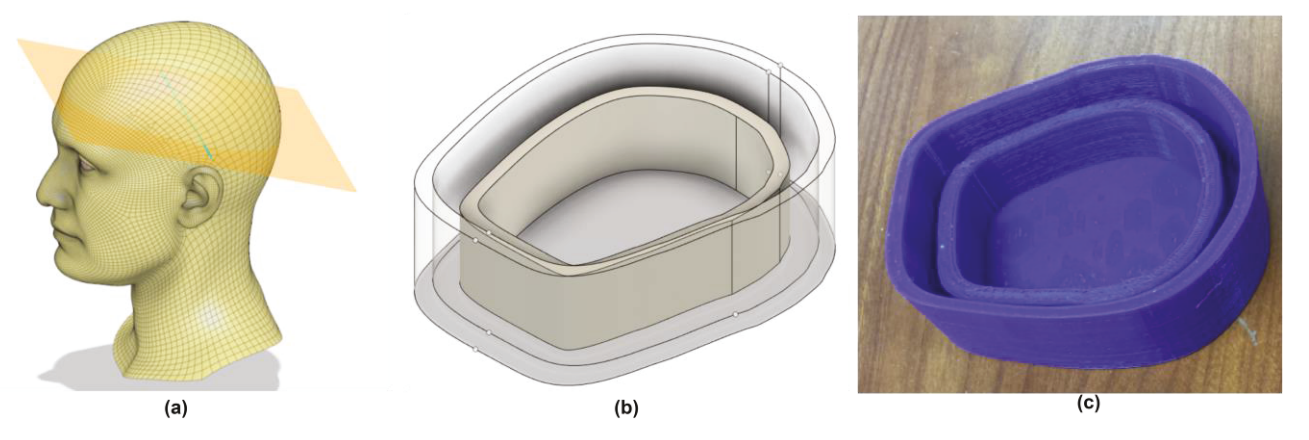


Figure 2.9. Design a 3D model of the multi-layered head phantom (a-b), and after it was printed by a 3D printer (c).

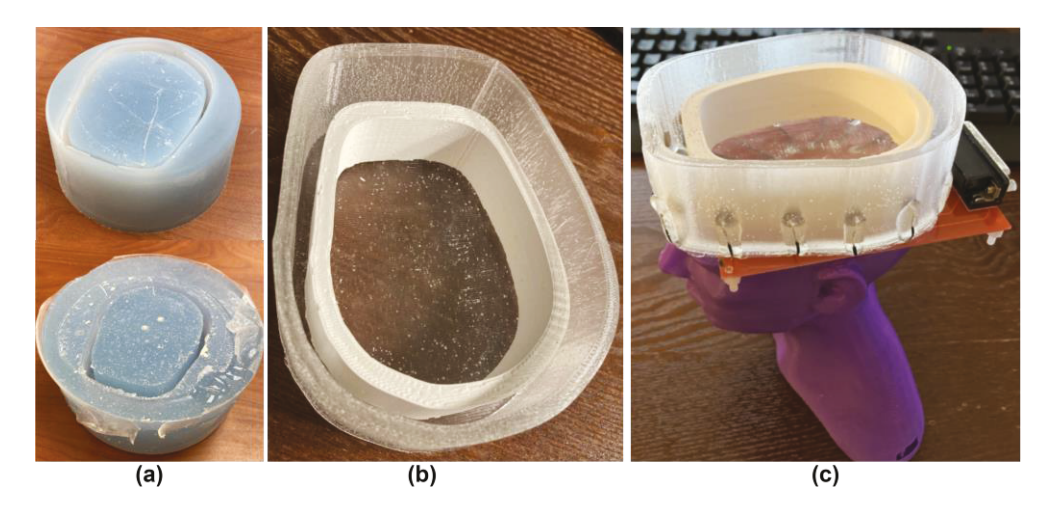


Figure 2.10. Molding the outer container and skull structure (a), after producing (b), and after attaching electrodes, wires, PCB board, and connector (c).

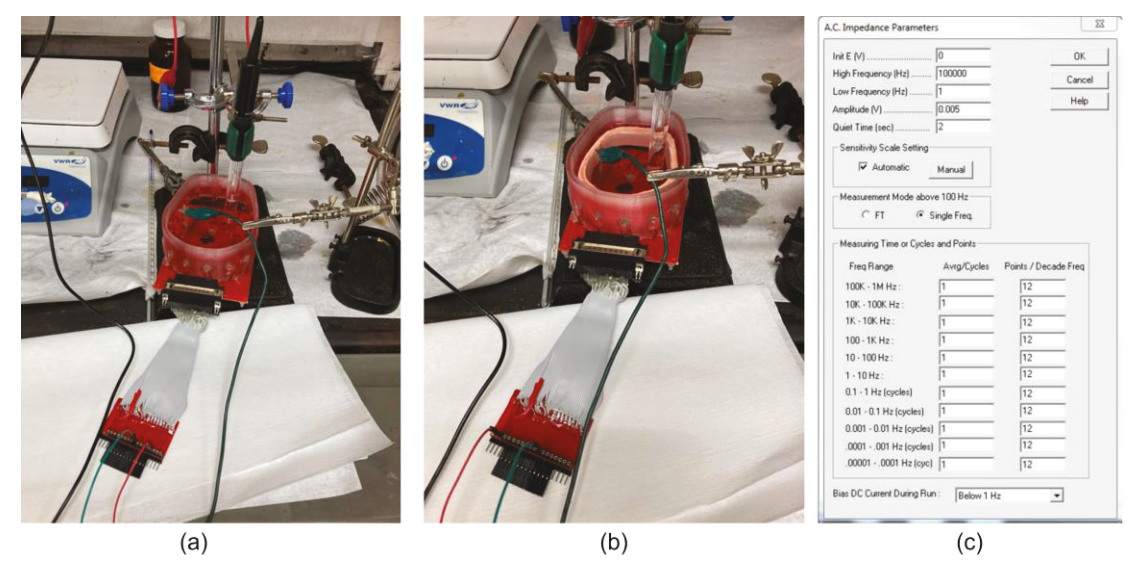


Figure 2.11. AC impedance measurement using a 3-electrode setup.

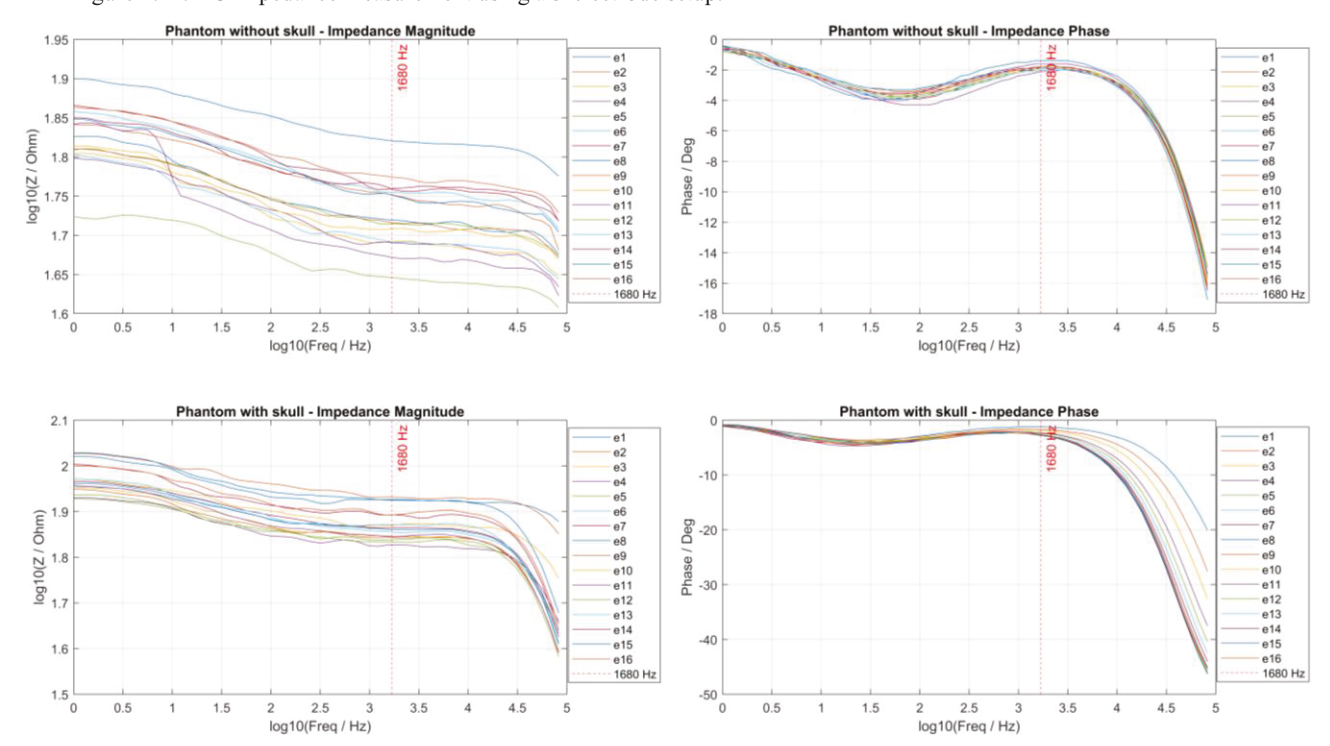


Figure 2.12. Electrodes AC impedance measurement results with PBS (10 millimoles) solutions.

Making a multi-layered head phantom is composed of four main steps, including drawing 3D-design of the head phantom; 3D-printing of the designed model; molding, producing the outer container and skull structure; and attaching electrodes and connector on the outer container (Figure 2.8). After getting an anatomical 3D model of a human head, a plane was made at the position where we planned to attach the round of electrodes if we did the experiment on humans (Figure 2.9 a). Based on the intersection between the plane and the 3D human head model, a 3D model of the outer container and skull structure were drawn after scaling the dimension to half of the real human head dimension (Figure 2.9 b). A 3D printer was used to print out the design, and its results are shown in Figure 2.9 (c). Polytek PlatSil 73-20 Silicon Rubber was used to make molds of the 3D printing models (Figure 2.10 a). With the outer container case, we used the Polytek Poly-Optic 1730 Clear Urethane Resin to produce it, which is displayed in Figure 2.10 (b). While with

the skull structure, we chose dental-grade plaster (Lab Stone Type III, Plaster Guys Co., Glenside, PA) as the skull-mimicking material. The 0.01 Mol of Phosphate Buffered Saline was mixed with plaster powder with a 1:1 ratio, followed by thorough stirring. After the plaster solution was filled into the mold, a vibration was used to remove the bubbles. The plaster-skull structure was taken out after coagulation, as shown in Figure 2.10 (b). Electrodes, electrical wires, a simple Printed-Circuit-Board (PCB), and a DB-25 connector were attached to the phantom. The complete version of the head phantom, which was placed on its base, is presented in Figure 2.10 (c).

After making the head phantom, we need to test the AC impedances of electrodes attached to the phantom. The AC impedance measurement using a 3-electrodes setup is shown in Figure 2.11, therein Figure 2.11(a) displays the experiment setup with a phantom that did not contain the skull structure, while Figure 2.11(b) shows the skull structure was attached to the phantom when executed the measurements. Experiments configurations were set with the numbers shown in Figure 2.11(c). We used the PBS solution (10 millimoles) as an electrolyte to simulate the brain and scalp tissues in this case. The purpose of this testing is to make sure that the connections between all electrodes, electrical wires, and connectors are made properly. Figure 2.12 shows that the impedances of all electrodes have the same value ranges of impedance magnitudes and phases. In comparison between the two top graphs, which are the results of a phantom without a skull structure, and the two bottom graphs, which are the results of a phantom with a skull structure, we can realize the increased impedances when the presents of the skull structure inside the phantom. The phase graphs also show that the impedance of electrodes mainly contains the resistance while the electrical reactance is negligible since the phase values at 1680 Hz are small (vertical red lines).

3. EXPERIMENT SETUP

The EIT prototype board was enclosed in a metal box so that it was protected from any physical impacts and electrostatic discharge when handling the experiments. Besides, the metal box also acts as a Faraday cage that can limit the noise that could be arisen from external conditions. Figure 3.1 shows the experimental setup of our EIT system with 16 electrodes head phantom. A DB25 cable was used to connect between the 16 electrodes head phantom and the inputs channels of the EIT board. A computer was connected to the EIT board by a USB connection to control the board and transfer the data. An 18V DC power supply also needs to feed into the EIT board to provide the power for the system. We would put a plastic object inside the head phantom in different positions to evaluate our EIT system. To visualize the comparison between the reconstruction images and the read head phantom with an object inside, we used a small USB webcam to capture the picture at the time of running the measurements. Graphic User Interface (GUI) software was developed to display the results, set up the system configurations, and control the operation of the system.

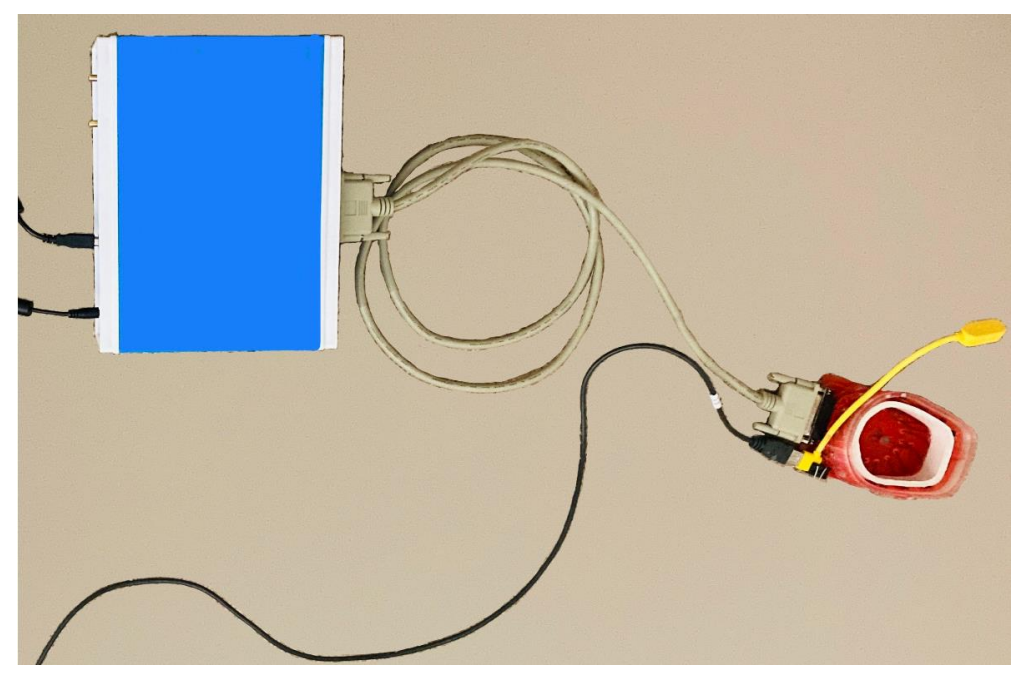


Figure 3.1. Experiment setup of EIT system with 16 electrodes head phantom.

4. RESULTS

Figure 3.1 shows the Graphic User Interface (GUI) software that was developed for controlling the EIT system and displaying experiment results. The picture captured from the USB webcam was displayed on the right panel of the GUI. The bottom right panel was used to plot a data channel after detecting the beginning point and end point of the data set that would help to determine whether the data acquisition worked well or not visually. The EIT reconstruction image was shown at the center panel of the GUI. With the EIT reconstruction image and the webcam-captured image dually displayed on the GUI, we could easily compare our EIT reconstruction image with the position of the plastic object inside the head phantom. The GUI's right panel was used to set the EIT system configurations, while the bottom panel was used to control the operation of the system.

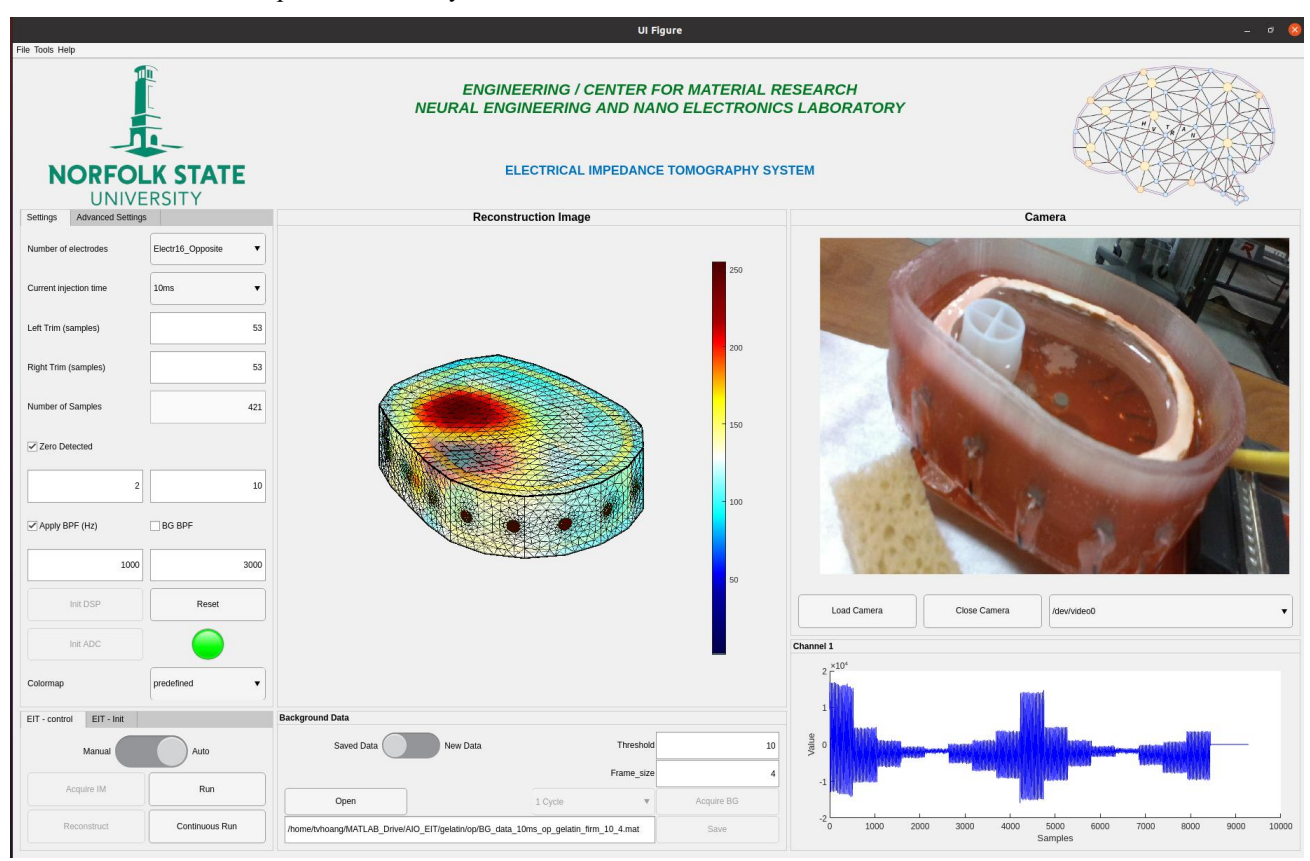


Figure 4.1. Graphic User Interface software.

Based on Figure 4.1 of the Graphic User Interface and Figure 3.1 of the experimental setup of the EIT system, we can imagine the whole system's operation processes. In the first step, on GUI, the user can set up the system configurations, like the number of electrodes and current injection method, ADC operation mode, sampling rate, etc., by inputting the parameters. Then back-end software will set up all parameters related to the software on the PC and send the hardware setup parameters to the EIT board via a USB connection. After finishing the hardware configuration on the EIT board, the board will send feedback to GUI to inform that the system is ready to do the measurement. In the second step, the user clicks on the RUN button to demand the system's operation. Control signals will be sent to the EIT board via the USB connection to start the electrical current injection and acquire the data on electrodes. At the same time, a picture of the head phantom will be captured to display on GUI's camera panel. The raw data, which is received from the EIT board, will go through the preprocessing steps described in section 2.2 before being fed into the EIT reconstruction algorithm. The reconstruction image will be shown on GUI's reconstruction image panel for the first time to compare with the webcam-captured picture. In the third step, some adjustments need to be made, both related to software configurations on the PC and hardware on the EIT board, to config the system's highest efficient operation based on the specific experimental conditions. Figure 4.2 shows the experimental results of 4 positions of the plastic object inside the head phantom, in companion with webcam-captured pictures. In comparison with the simulation results in Figure 4.3,

the location and the shape of the region of interest (ROI) are similar. These results demonstrated our EIT system's high accuracy and efficiency in brain imaging applications.

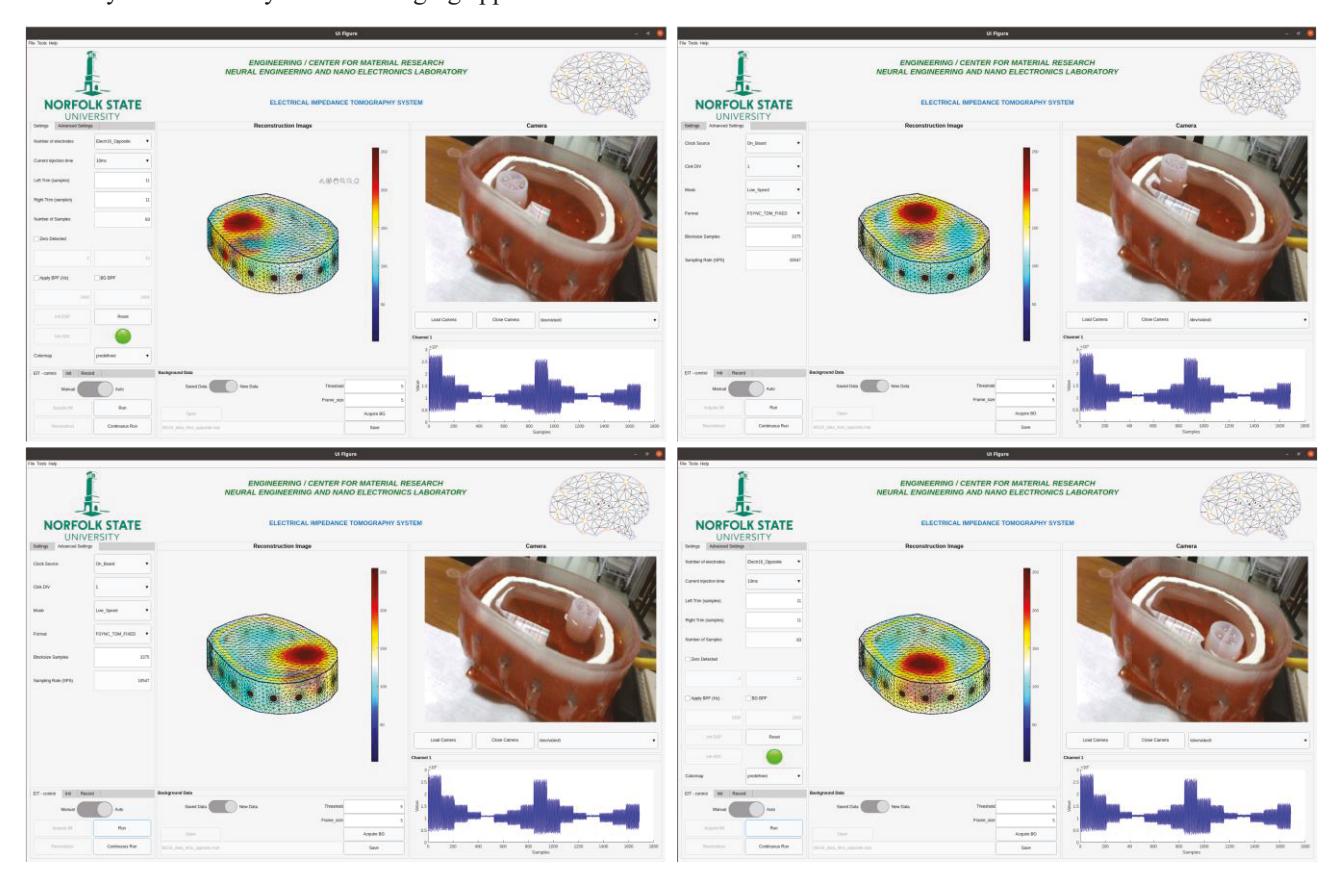


Figure 4.2. Reconstruction images of a head phantom with an object at four different positions.

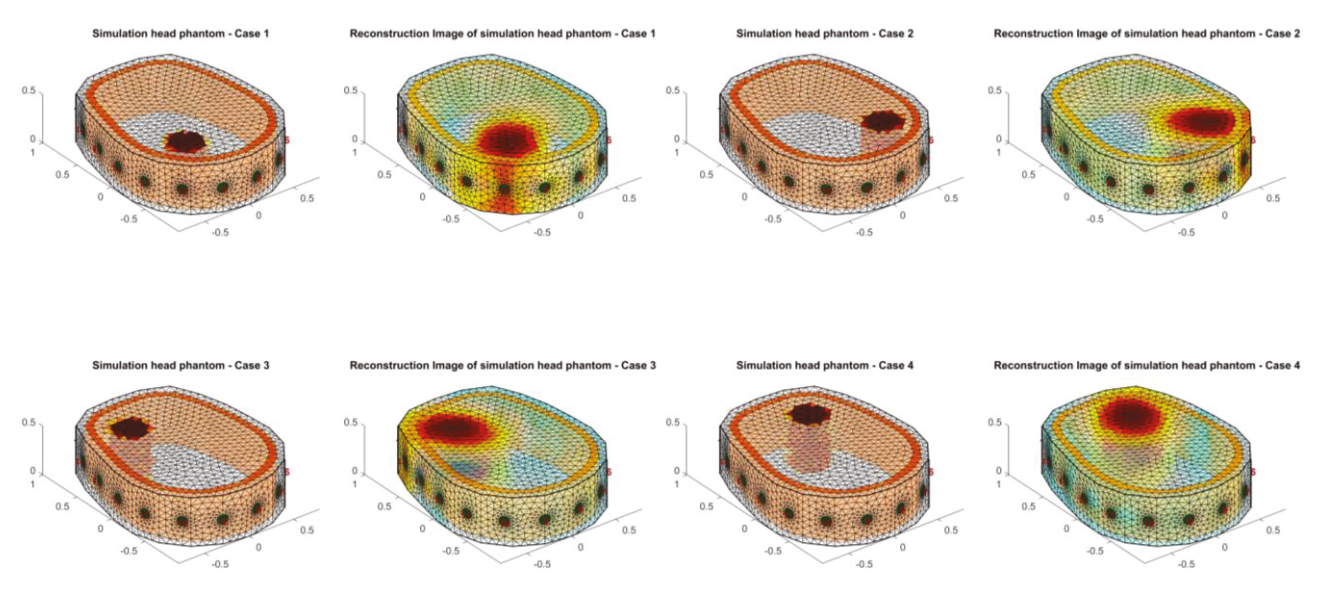


Figure 4.3. Simulation results of four object positions inside the head phantom.

5. DISCUSSIONS AND CONCLUSIONS

In this study, we presented the completed EIT system that demonstrated highly accurate and efficient operations. The electronic prototype board contains a high-quality electrical current source, and a high sampling rate and bit-resolution ADC were shown and evaluated to confirm the accuracy of the hardware components. In addition to high-accuracy hardware parts, the preprocessing data also dominated the system's efficiency. Head phantom, which has the anatomical geometry and high-resistive skull inside, was introduced with specific steps of fabrication and verification. The entire EIT system setup was shown, and the GUI software also demonstrated the system's controls and operations very conveniently and flexibly. Experiment results compared with the simulation results of the different object positions inside the head phantom confirm the efficiency of our system and the potential of our EIT system in brain imaging applications.

ACKNOWLEDGMENT

This work was partially supported by the National Science Foundation under projects (1831962 and 1827847).

REFERENCES

- [1] D. Holder, Electrical Impedance Tomography Methods, History and Applications, 1st ed. CRC Press, 2004.
- [2] X.-Y. Ke *et al.*, "Advances in electrical impedance tomography-based brain imaging," *Military Medical Research*, vol. 9, no. 1, p. 10, Feb. 2022, doi: 10.1186/s40779-022-00370-7.
- [3] "Dräger PulmoVista® 500 | Draeger." https://www.draeger.com/en_aunz/Products/PulmoVista-500 (accessed Mar. 11, 2023).
- [4] "Electrical Impedance Tomography (EIT) Device LuMonTM," *Sentec*. https://www.sentec.com/electrical-impedance-tomography/ (accessed Mar. 11, 2023).
- [5] K. Boone, A. M. Lewis, and D. S. Holder, "Imaging of cortical spreading depression by EIT: implications for localization of epileptic foci," *Physiol. Meas.*, vol. 15, no. 2A, p. A189, May 1994, doi: 10.1088/0967-3334/15/2A/024.
- [6] L. Fabrizi *et al.*, "Factors limiting the application of electrical impedance tomography for identification of regional conductivity changes using scalp electrodes during epileptic seizures in humans," *Physiol. Meas.*, vol. 27, no. 5, p. S163, Apr. 2006, doi: 10.1088/0967-3334/27/5/S14.
- [7] A. Romsauerova, A. McEwan, and D. S. Holder, "Identification of a suitable current waveform for acute stroke imaging," *Physiol. Meas.*, vol. 27, no. 5, p. S211, Apr. 2006, doi: 10.1088/0967-3334/27/5/S18.
- [8] T. Dowrick, C. Blochet, and D. Holder, "In vivo bioimpedance measurement of healthy and ischaemic rat brain: implications for stroke imaging using electrical impedance tomography," *Physiol. Meas.*, vol. 36, no. 6, p. 1273, May 2015, doi: 10.1088/0967-3334/36/6/1273.
- [9] F. Fu *et al.*, "Use of Electrical Impedance Tomography to Monitor Regional Cerebral Edema during Clinical Dehydration Treatment," *PLOS ONE*, vol. 9, no. 12, p. e113202, Dec. 2014, doi: 10.1371/journal.pone.0113202.
- [10] H. Li *et al.*, "Unveiling the development of intracranial injury using dynamic brain EIT: an evaluation of current reconstruction algorithms," *Physiol. Meas.*, vol. 38, no. 9, p. 1776, Aug. 2017, doi: 10.1088/1361-6579/aa8016.
- [11] X. Liu *et al.*, "An iterative damped least-squares algorithm for simultaneously monitoring the development of hemorrhagic and secondary ischemic lesions in brain injuries," *Med Biol Eng Comput*, vol. 57, no. 9, pp. 1917–1931, Sep. 2019, doi: 10.1007/s11517-019-02003-z.
- [12] H. Tran, V. Pham, T. Le, and H. Yoon, "Signal processing to improve speed and accuracy of electrical impedance tomography imaging," in *Nano-, Bio-, Info-Tech Sensors and Wearable Systems*, Mar. 2021, vol. 11590, pp. 88–95. doi: 10.1117/12.2585224.
- [13] Texas Instruments, "Quad/Octal, Simultaneous Sampling, 24-Bit Analog-to-Digital Converters", SBAS367F June 2007 Revised February 2011.